Catalysis Communications 32 (2013) 62–66

Contents lists available at SciVerse ScienceDirect

Catalysis Communications

journal homepage: www.elsevier.com/locate/catcom

Short Communication

Synthesis of menthols from citral on $Ni/SiO_2–Al_2O_3$ catalysts

A.F. Trasarti, A.J. Marchi, C.R. Apesteguía *

Catalysis Science and Engineering Research Group (GICIC), INCAPE, UNL-CONICET. Santiago del Estero 2654. (3000) Santa Fe, Argentina

ARTICLE INFO

Article history:
Received 17 October 2012
Received in revised form 14 November 2012
Accepted 30 November 2012
Available online 7 December 2012

Keywords:
Menthol synthesis
Ni catalysts
Citral
Fine chemistry

ABSTRACT

The one-pot synthesis of menthols from citral was studied on $Ni/SiO_2–AlO_3$ catalysts containing 3.6%, 8.8% and 11.4% Ni. The yield of menthols increased with the amount of Ni up to 94% on $Ni(11.4\%)/SiO_2–AlO_3$, reflecting the diminution of byproducts formation via acid-catalyzed reactions. The sample deactivation was studied by performing two consecutive catalytic tests. Results showed that $Ni(11.4\%)/SiO_2–AlO_3$ was a stable, active, and highly selective catalyst because it contained the appropriate density and strength of bifunctional acid/Ni^0 active sites to efficiently promote the hydrogenation/isomerization pathway involved in the reaction network while avoiding coke formation.

1. Introduction

Menthol is used extensively in pharmaceuticals, cosmetics and toothpastes, as well as in cigarettes. Of the four pairs of optical menthol isomers, (±)-menthol, (±)-isomenthol, (±)-neomenthol, and (±)-neoisomenthol, only (−)-menthol has the characteristic peppermint odor and exerts a unique cooling sensation on the skin and mucous membranes. Most of the menthol used worldwide is obtained by separation of *Mentha* piperita essential oil, but it is also produced synthetically. Symrise and Takasago are currently the only major producers of synthetic (−)-menthol. In the Symrise process [1], thymol is hydrogenated to racemic (±)-menthols which are separated by a crystallization process to obtain (−)-menthol. The Takasago process [2] produces (−)-menthol from myrcene using an asymmetric synthesis technology.

Other synthetic routes to produce menthols from more readily reliable raw materials have been lately investigated. In particular, we reported for the first time in 2004 the one-pot synthesis of menthols from citral [3]. Citral is an attractive renewable raw material that may be obtained by distillation of essential oils, such as lemongrass oil, which contains ca. 70–80% citral. One-pot synthesis of menthols directly from citral is not easily achieved because it requires to develop bifunctional metal/acid catalysts with the ability to selectively promote the following consecutive reaction steps (Scheme 1): (i) hydrogenation of citral to citronellal; (ii) cyclization of citronellal to isopulegols; and (iii) hydrogenation of isopulegols to menthols. The individual reactions involved in the citral-to-menthols reaction network showed in Scheme 1 have been extensively studied, but often the objectives of these studies were not directed to the synthesis of menthols. For example, the selective hydrogenation of citral was investigated for producing either nerol/geraniol [4] or citronelol [5]; few papers have studied the citral hydrogenation to citronellal [6]. The citronellal cyclization to isopulegol has been carried out by using liquid [7] and solid [8] acid catalysts while the direct synthesis of menthols from citronellal was investigated on Ru [9], Pt [10] and Cu [11] catalysts. In contrast, few papers have investigated the direct synthesis of menthols from citral [12–15]. In previous works [3,13] we studied this later reaction on noble (Pt, Pd, Ir) and nonnoble (Ni, Co, Cu) metals supported over different solid acids (ZnO/SiO_2, CsHPA, zeolites, Al-MCM-41). The best catalyst was Ni(8%)/Al-MCM-41 that yielded more than 90% menthols at 2026 kPa. In this work we have extended these studies to investigate the synthesis of menthols from citral on $Ni/SiO_2–Al_2O_3$ catalysts containing different amounts of Ni. The goal was to explore the development of $Ni/SiO_2–Al_2O_3$ catalysts showing at least similar catalytic performance than Ni(8%)/Al-MCM-41, taken into account that $Ni/SiO_2–Al_2O_3$ catalysts are more economic and easier to prepare. To achieve this objective we need to optimize the catalyst performance by tuning the density and strength of bifunctional Ni^0/acid surface sites that selectively promote the hydrogenation/isomerization/hydrogenation pathway involved in the reaction network depicted in Scheme 1.

2. Experimental

2.1. Catalyst preparation

Silica–alumina supported catalysts were prepared by incipient-wetness impregnation at 303 K. Aqueous Ni nitrate solutions ($Ni(NO_3)_2.6H_2O$ Anedra ACS) were used for impregnating Ni on a commercial $SiO_2–Al_2O_3$ powder (Sigma-Aldrich 135 grade, Si/Al =

* Corresponding author. Tel.: +54 342 4555279; fax: +54 342 4531068.
E-mail address: capesteg@fiq.unl.edu.ar (C.R. Apesteguía).
URL: http://www.fiq.unl.edu.ar/gicic/ (C.R. Apesteguía).

1566-7367/$ – see front matter © 2012 Elsevier B.V. All rights reserved.
http://dx.doi.org/10.1016/j.catcom.2012.11.030

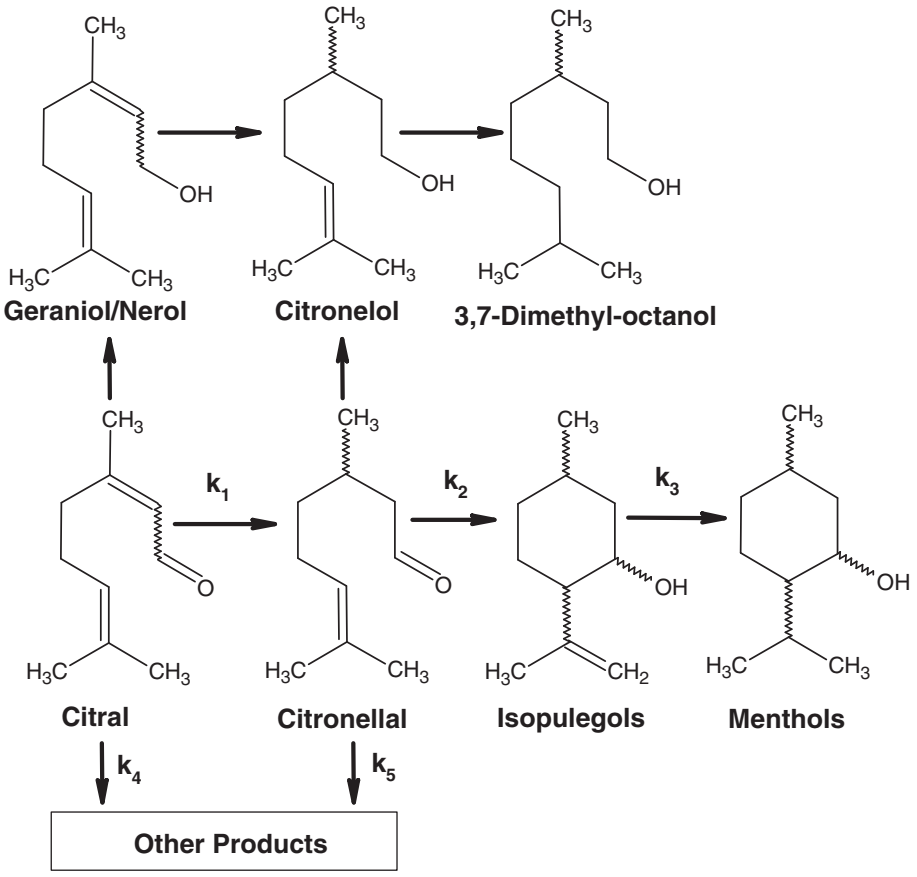

Scheme 1. Synthesis of menthols from citral.

16). The impregnated samples were dried overnight at 363 K, then heated in air (60 cm^3/min STP) at 10 K/min to 673 K and kept at this temperature for 2 h. Three samples containing 3.6, 8.8 and 11.4 % Ni were prepared and are identified here as Ni/SA-I, Ni/SA-II and Ni/SA-III, respectively.

2.2. Catalyst characterization

BET surface areas (S_g), mean pore diameter (dp), and pore-size distribution were measured by N_2 physisorption at 77 K using the BET method and Barret–Joyner–Halender (BJH) calculations in a Micromeritics Accusorb 2100E sorptometer. Elemental compositions were measured by atomic absorption spectroscopy (AAS) in a Perkin-Elmer 3110 espectrometer. Powder X-ray diffraction (XRD) patterns were collected in the range of $2\theta = 5–80°$ using a Shimadzu XD-D1 diffractometer and Ni-filtered Cu Kα radiation. Oxide crystallite sizes were calculated using the Debye–Scherrer equation.

The accessible Ni fraction was determined by chemisorption of hydrogen. Volumetric adsorption experiments were performed at 298 K in a conventional vacuum unit. Catalysts were reduced in H_2 at 673 K for 2 h and then outgassed 2 h at 773 K prior to performing gas chemisorption experiments. Strong hydrogen uptake was determined using the double isotherm method as detailed previously [16].

The temperature programmed reduction (TPR) experiments were performed in a Micromeritics AutoChem II 2920, using 5% H_2/Ar gaseous mixture at 60 cm^3/min STP. The sample size was 150 mg. Samples were heated from 298 to 1050 K at 10 K/min. Since water is formed during sample reduction, the gas exiting from the reactor was passed through a cold trap before entering the thermal conductivity detector.

Sample acidity was determined by temperature-programmed desorption (TPD) of NH_3 preadsorbed at 373 K. Samples (150 mg) were treated in He (60 cm^3/min STP) at 773 K for 0.5 h and then exposed to a 1% NH_3/He stream for 40 min at 373 K. Weakly adsorbed NH_3 was removed by flushing with He at 373 K during 2 h. Temperature was then increased at 10 K/min and the NH_3 concentration in the effluent was measured by mass spectrometry in a Baltzers Omnistar unit.

2.3. Catalytic activity

The liquid-phase hydrogenation of citral (Aldrich, 98%) was studied in a Parr 4843 reactor at 343 K, using toluene (Cicarelli, p.a.) as solvent. The autoclave was loaded with 150 ml of solvent, 2 ml of citral and 1 g of catalyst. Prior to catalytic tests, samples were activated ex-situ in hydrogen (50 ml/min) for 1 h at 723 K and loaded immediately to the reactor under inert atmosphere. The reaction system was heated to 343 K at 2 K/min, and the pressure was then rapidly increased to 2026 kPa with H_2. Product concentrations were determined by ex-situ gas chromatography using a Agilent 6850 GC chromatograph equipped with flame ionization detector and a 30 m Supelco α-DEX capillary column. The product analysis and carbon balance were performed using n-dodecane as an external standard. Data were collected every 20–30 min for 130–220 min. Interparticle and intraparticle diffusional limitations were verified as negligible. Conversion of citral was calculated as $X_{Cit} = (C^0_{Cit} - C_{Cit})/C^0_{Cit}$, where C^0_{Cit} is the initial concentration of citral and C_{Cit} is the citral concentration at time t. Selectivities (S_j, mol of product j/mol of citral reacted) were calculated as $S_j = C_j/(C^0_{Cit} - C_{Cit})$. Yields ($\eta_j$, mol of product j/mol of citral fed) were calculated as $\eta_j = S_j X_{Cit}$. The main reaction products detected were citronellal, isopulegols, (±)-menthols, (±)-neomenthols, (±)-isomenthols and (±)-neoisomenthols. The yield of other products not detected by gas chromatography was calculated as $\eta_{Others} = 1 - \Sigma_j \eta_j$.

Table 1
Catalyst characterization.

Catalyst	Ni loading [a] (%)	Sg (m^2/g)	Vp (cm^3/g)	Average pore diameter D_p (Å)	NiO crystallite size [b] (nm)	H_2 uptake (μmol/g Ni)	Ni dispersion (%)	TPR			TPD of NH_3 n_a (μmol/g)
								T_m (K)	H_2 consumption ($\mu mol/g_{cat}$)		
									LT peak	HT peak	
SiO_2–Al_2O_3	–	541	0.77	57	–	–	–	–	–	–	443
Ni/SA-I	3.6	540	0.72	57	-	221	2.6	591, 795	237	261	400
Ni/SA-II	8.8	465	0.67	53	10	148	1.7	620, 812	606	288	329
Ni/SA-III	11.4	405	0.53	52	14	123	1.2	679, 806	1325	194	258

[a] Determined by AAS.
[b] Determined by XRD.

3. Results and discussion

3.1. Catalyst characterization

The physical properties of SiO_2–Al_2O_3, Ni/SiA-I, Ni/SiA-II and Ni/SiA-III together with the results of sample characterization are given in Table 1. The BET surface area of the SiO_2–Al_2O_3 support (541 m^2/g) decreased with the metal content up to 405 m^2/g for Ni/SiA-III, probably reflecting a partial blockage of the porous structure by the metal. The sample pore volume diminished with the % Ni on the support, from 0.77 cm^3/g (SiO_2–Al_2O_3) to 0.53 cm^3/g (Ni/SiA-III). Nevertheless, the average pore diameter did not change significantly with the Ni loading (Table 1).

XRD patterns of calcined Ni-containing samples are shown in Fig. 1. NiO (ASTM 4-835) was identified on all the samples, but the XRD signal was too weak for determining with exactitude the NiO particle size on Ni/SiA-I. The mean NiO crystallite sizes were 10 nm and 14 nm for Ni/SiA-II and Ni/SiA-III, respectively. The hydrogen uptake of reduced samples (Table 1) decreased from 221 μmol/g Ni (Ni/SiA-I) to 123 μmol/g Ni (Ni/SiA-III) which is consistent with the NiO particle size determined from the diffractograms of Fig. 1.

The TPR profiles of Ni/SiA catalysts exhibited two reduction peaks (Fig. 2). The low-temperature peak (LT peak) appeared in the 500–700 K region and would represent the direct reduction of NiO to metallic nickel, taken into account that the reduction temperature of bulk nickel oxide is 503 K [17]. As shown in Table 1, the maximum (T_m) of the LT peak increased with the NiO crystallite size. This shift of T_m with the NiO crystallite size is consistent with the unreacted shrinking core model predictions for non-porous metal oxides reduction. Previous work [18,19] has effectively furnished convincing experimental evidence for the dependence of T_m on particle size by modeling TPR profiles of different-sized particles of NiO with the unreacted core model. In contrast, the T_m values corresponding to the high-temperature peak (HT peak) in Fig. 2 were similar, i.e. T_m did not change significantly with the NiO particle size (Table 1). Moreover, the H_2 consumptions for the HT peak did not increase with the Ni loading on the sample. Other authors [20] have also observed that the TPR profiles of NiO/SiO_2Al_3 consist of two reduction peaks, and they have proposed that the HT peak represents the reduction of Ni^{2+} species formed by partial cation exchange with the support during the impregnation. The presence of Ni^{2+} species in strong interaction with silica and alumina may explain that in Table 1 the T_m and H_2 consumption values corresponding to HT peaks do not depend on NiO crystallite size.

The TPD curves of Ni/SiA catalysts are shown in Fig. 3. The NH_3 surface densities for acid sites (n_a, μmol/g) were obtained by deconvolution and integration of TPD traces and are presented in Table 1. All the samples exhibited a single asymmetric NH_3 band with a maximum at around 545–580 K. The concentration of surface acid sites decreased with the amount of Ni on the sample, suggesting a partial coverage of surface acid sites by the metal. In a previous paper [21] we have characterized the acidity of the SiO_2–Al_2O_3 sample used in this work by FTIR of adsorbed pyridine and observed that it contains Brønsted and Lewis acid sites. We determined that the Lewis/Brønsted acid sites ratio was close to 3.

3.2. Catalyst activity and selectivity

Fig. 4 shows the evolution of citral conversion and yields on Ni/SiA catalysts as a function of parameter $t\,W/n^0_{cit}$, where t is the reaction time, W is the catalyst weight, and n^0_{cit} is the initial moles of citral. The local slopes of the curves in Fig. 4 give the rate of formation of each product at a specific value of citral conversion and reaction time. The initial

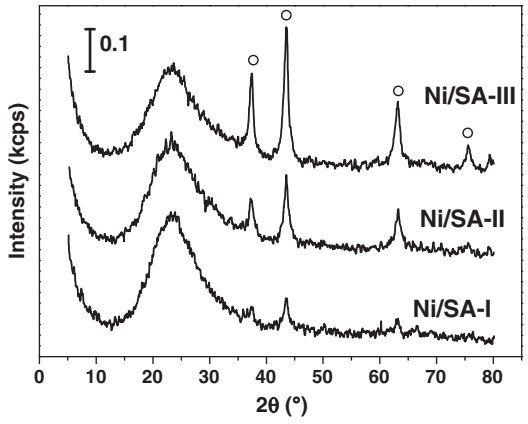

Fig. 1. X-ray diffractograms of Ni/SiO_2–Al_2O_3 samples. ○, NiO.

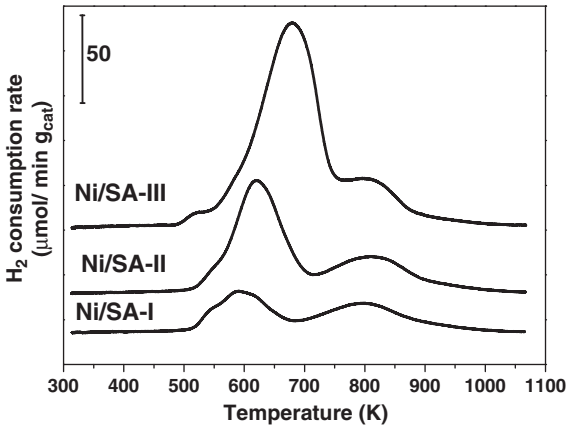

Fig. 2. TPR characterization of Ni/SiO_2–Al_2O_3 samples.

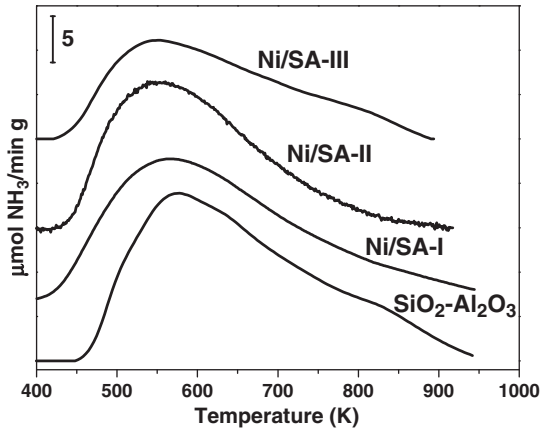

Fig. 3. TPD profiles of NH_3.

citral conversion rates (r^0_{cit}, mol/h g_{cat}) determined from the curves of Fig. 4 are presented in Table 2. The r^0_{cit} values increased with the %Ni on the catalyst, from 0.033 (Ni/SiA-I) to 0.078 mol/h g_{cat} (Ni/SiA-III). Citral was totally converted to citronellal on all the catalysts after 30–45 min but the concentration of citronellal remained relatively low during the progress of the reaction because it was rapidly converted to isopulegols. Actually, the citronellal concentration at the beginning of the reaction was negligible on Ni/SiA-I but increased with the %Ni on the sample showing clearly on Ni/SiA-III the typical curve of primary products in consecutive reactions that presents a maximum concentration with the reaction time (Fig. 4). This result reflects the fact that the k_1/k_2 kinetic constant ratio (see Scheme 1) increases with the %Ni on the sample. In fact, k_1 (hydrogenation of citral to citronellal) increases with the amount of metal sites while k_2 (isomerization of citronellal to isopulegols) diminishes because surface acid sites are increasingly covered when the Ni loading is increased (Table 1). Isopulegols were then completely converted to menthols after 210, 150 and 100 min on Ni/SiA-I, Ni/SiA-II and Ni/SiA-III, respectively, reflecting the increase of the isopulegol hydrogenation kinetic constant (k_3, Scheme 1) with the amount of Ni on the sample.

The yield of menthols increased with the amount of Ni on the catalyst, from 67% (Ni/SiA-I) to 94% (Ni/SiA-III) (Table 2). This result would essentially reflect the diminution of byproducts formation via acid-catalyzed reactions. Fig. 4 shows, in fact, that Ni/SiA-I formed at the beginning of the reaction significant amounts of "other" products that remain then approximately constant with the progress of the reaction. Formation of these "other" products at the beginning of the reaction suggests that they are essentially produced from citral and citronellal, probably via parallel reactions on the acid sites of SiO_2–Al_2O_3 support (reaction pathways involving kinetic constants k_4 and k_5 in Scheme 1). In order to confirm this assumption, we carried out the citral conversion reaction on SiO_2–Al_2O_3 in H_2 at 343 K and 2025 kPa (the catalytic run is not shown here) and observed that citral was converted to "other" products which supported the assumption that coke is formed from citral conversion reactions taking place on the acid support. The diminution of the acid site density with the amount of Ni on the sample (Fig. 3 and Table 1) would explain then that the byproduct formation decreased from Ni/SiA-I (33%) to Ni/SiA-III (6%) (Table 2). Finally, we want to note that Ni/SiA-I sample was also tested at 506 and 1013 kPa in order to investigate the effect of pressure on catalyst selectivity. The menthols yields obtained at 506 and 1013 kPa on Ni/SiA-I were 54% and 63%, respectively; i.e. similar menthol yields were obtained on this catalyst at 1013 and 2025 kPa.

In summary, our results in Table 2 and Fig. 4 show that the activity and selectivity for the formation of menthols from citral on Ni/SiO_2–Al_2O_3 samples are significantly improved by increasing the amount of Ni on the sample because: i) the citral and isopulegol hydrogenation rates increase with the surface concentration of Ni^0 active sites; ii) the increasing coverage of the support by Ni diminishes the formation of undesirable byproducts on surface acid sites. Regarding the distribution of menthol isomers, Table 2 shows that the composition of the menthol mixture was similar on all the Ni/SiA samples, containing 70% of (±)-menthols, 20–21% of (±)-neomenthols, 5–6% of isomenthols, and 3–4% of (±)-neoisomenthols.

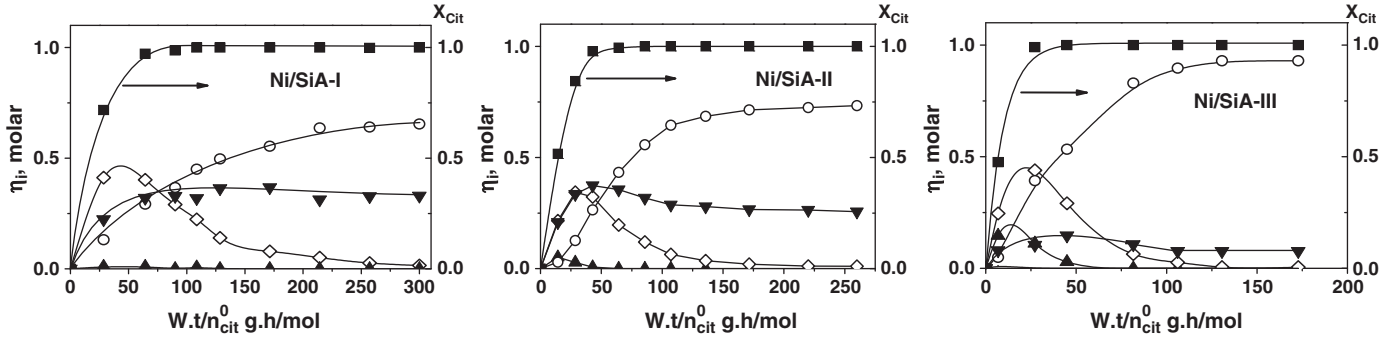

Fig. 4. Catalytic results: citral conversion (X_{Cit}) and yields (η_i). ▲ citronellal, ◇ isopulegols, ○ menthols, ▼ others. [T = 343 K, P = 2025 kPa, Solvent: toluene, W_{cat} = 1 g].

Table 2
Catalytic results.

Catalyst	r^0_{cit} [a] (mol/h g_{cat})	Reaction length (min)	X_{cit} [b]	Yields (η_i, molar %) [b]			Mentol isomer distribution (%) [b]			
				Isopulegols	Menthols	Others	(±)-Menthols	(±)-Neomenthols	(±)-Isomenthols	(±)-Neoisomenthols
Ni/SA-I	0.033	210	100	0	67	33	70	21	6	3
Ni/SA-II	0.048	180	100	0	74	26	70	21	5	4
Ni/SA-III	0.078	120	100	0	94	6	70	20	6	4

T = 343 K, P = 2026 kPa, W = 1 g, citral/toluene = 2:150 (ml)
[a] Initial citral conversion rate.
[b] Determined at the end of catalytic runs.

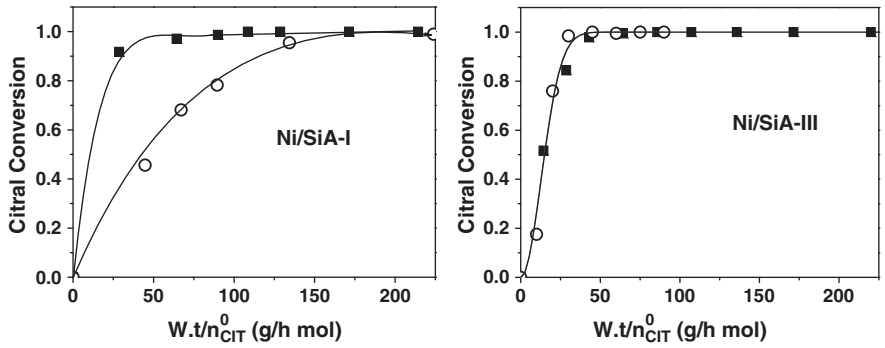

Fig. 5. Consecutive in situ catalytic runs to evaluate catalyst deactivation. ■ First runs; ○ second runs. Reaction conditions as in Fig. 4.

3.3. Catalyst deactivation

We studied the deactivation of $Ni/SiO_2–Al_2O_3$ samples by performing two consecutive catalytic tests without stopping the run. The procedure was as follows: Immediately after isopulegols were completely transformed to menthols in a standard run at 2026 kPa, we introduced to the reactor (without opening it) the same amount of initial moles of citral, n^0_{cit}, and performed a second consecutive run. Fig. 5 shows the evolution of the conversion of citral for the two consecutive catalytic runs on Ni/SiA-I and Ni/SiA-III samples. The initial citral conversion rate on Ni/SiA-I in the second run was clearly lower as compared to that in the first run. As a consequence, the reaction length required for achieving the complete citral conversion on Ni/SiA-I was 35 minutes in the first run and 120 minutes in the second run. These results indicated that the Ni/SiA-I catalyst was partially deactivated during the first catalytic run, probably because of coke formation. In contrast, Fig. 5 shows that the evolutions of citral conversion on Ni/SiA-III were practically the same for both consecutive catalytic tests, thereby showing that the catalyst deactivation during the progress of the reaction was negligible. Thus, the increase of the %Ni on the sample not only improved the catalyst activity and selectivity but also had a positive effect on catalyst stability. Probably, the buildup of carbonaceous deposits on $Ni/SiO_2–Al_2O_3$ catalysts is mainly related to the formation of byproducts at the beginning of reaction, as detailed above. This could explain the greater stability observed in Fig. 5 for Ni/SiA-III sample because the byproduct formation decreases with the amount of Ni on the sample (Table 2).

On the other hand, the yields of menthols at the end of second runs on Ni/SiA-I ($\eta_{menthol} = 84\%$) and Ni/SiA-II ($\eta_{menthol} = 86\%$) were higher than those obtained at the end of first runs (Table 2), reflecting the diminution of byproduct formation during the second runs. These results are consistent with the preferential formation of coke precursors during the first runs on the strongest acid sites of the support that are also responsible for the conversion of citral and citronellal to byproducts at the beginning of reaction (Scheme 1). Indeed, these strong acid sites of the support will be deactivated for the second catalytic run causing the diminution of byproduct formation and, consequently, improving the selectivity to menthols.

4. Conclusions

The activity, selectivity and stability of $Ni/SiO_2–Al_2O_3$ catalysts for the one pot synthesis of menthols from citral can be optimized by tuning the density and strength of bifunctional Ni^0/acid surface sites that selectively promote the hydrogenation/isomerization/hydrogenation pathway involved in the reaction network. The strong acidity of $SiO_2–Al_2O_3$ support catalyzes the conversion of citral and citronellal to undesirable byproducts thereby decreasing the catalyst selectivity to menthols. Thus, the Ni/SiA-I (3.6% Ni) catalyst produced 33% of byproducts and only 67% of menthols. The increase of the Ni loading increases the concentration of surface Ni^0 sites and simultaneously diminishes the sample acidity by partially blocking the access to the support acid sites. As a result, the citral and isopulegol hydrogenation rates increase while the acid-catalyzed byproducts formation diminishes with the amount of Ni which improves the selective formation of menthols. For example, the menthols yield was 74% on Ni/SiA-II (8.8% Ni) catalyst. The highest menthol yield (94%) was obtained on Ni/SiA-III (11.4% Ni) catalyst; this value is similar to the best yields reported in literature for the direct synthesis of menthols from citral on bifunctional metal/acid catalysts. The increase of the %Ni in $Ni/SiO_2–Al_2O_3$ catalyst has also a positive effect on catalyst stability, probably because the buildup of carbonaceous deposits is mainly related to the acid-catalyzed reactions forming byproducts from citral and citronellal that diminish with the amount of Ni on the sample.

Acknowledgements

The Authors thank the Universidad Nacional del Litoral (UNL), Consejo Nacional de Investigaciones Científicas y Técnicas (CONICET), and Agencia Nacional de Promoción Científica y Tecnológica (ANPCyT), Argentina, for the financial support of this work.

References

[1] J. Fleischer, K. Bauer, R. Hopp, DE 2109456, Harrmann & Reimer, 1971.
[2] M. Misono, N. Nojiri, Applied Catalysis 64 (1990) 1–30.
[3] A. Trasarti, A.J. Marchi, C.R. Apesteguía, Journal of Catalysis 224 (2004) 484–488.
[4] S. Recchia, C. Dossi, N. Poli, A. Fussi, L. Sordelli, R. Psaro, Journal of Catalysis 184 (1999) 1–4.
[5] G. Lafaye, T. Ekou, C. Micheaud-Especel, C. Montassier, P. Marecot, Applied Catalysis A: General 257 (2004) 107–117.
[6] U.K. Singh, M.A. Vannice, Journal of Catalysis 199 (2001) 73–84.
[7] P. Kocovský, G. Ahmed, J. Šrogl, A.V. Malkov, J. Steele, The Journal of Organic Chemistry 64 (1999) 2765–2775.
[8] Z. Yongzhong, N. Yuntong, S. Jaenicke, G.K. Chuah, Journal of Catalysis 229 (2005) 404–413.
[9] C. Milone, C. Gangemi, G. Neri, A. Pistone, S. Galvagno, Applied Catalysis A: General 199 (2000) 239–244.
[10] P. Mertens, F. Verpoort, A.N. Parvulescu, D. De Vos, Journal of Catalysis 243 (2006) 7–13.
[11] N. Ravasio, N. Poli, R. Psaro, F. Zaccheria, Topics in Catalysis 13 (2000) 195–199.
[12] P. Mäki-Arvela, N. Kumar, D. Kubicka, A. Nasir, T. Heikkilä, V.P. Lehto, R. Sjöholm, T. Salmi, D.Yu. Murzin, Journal of Molecular Catalysis A: Chemical 240 (2005) 72–81.
[13] A.F. Trasarti, A.J. Marchi, C.R. Apesteguía, Journal of Catalysis 247 (2007) 155–165.
[14] P. Virtanen, H. Karhu, G. Tothc, K. Kordas, J.P. Mikkola, Journal of Catalysis 263 (2009) 209–219.
[15] Y. Nie, S. Jaenicke, G.K. Chua, Chemistry - A European Journal 15 (2009) 1991–1999.
[16] A. Borgna, T.F. Garetto, C.R. Apesteguía, F. Le Normand, B. Moraweck, Journal of Catalysis 186 (1999) 433–441.
[17] J. Zielinski, Journal of Catalysis 76 (1982) 157–163.
[18] K.H. Tonge, Thermochimica Acta 74 (1984) 151–166.
[19] M.J.L. Ginés, C.R. Apesteguía, Latinam Applied Research 25 (1995) 215–221.
[20] A. Lewandowska, S. Monteverdi, M. Bettahar, M. Ziolek, Journal of Molecular Catalysis A: Chemical 188 (2002) 85–95.
[21] C.L. Padró, C.R. Apesteguía, Journal of Catalysis 226 (2004) 308–320.